3D printed metamaterial absorbers for midinfrared surface-enhanced spectroscopy

Cite as: Appl. Phys. Lett. **120**, 191703 (2022); https://doi.org/10.1063/5.0093332 Submitted: 28 March 2022 • Accepted: 02 May 2022 • Published Online: 11 May 2022

🗓 Albanie K. Hendrickson-Stives, 🗓 Lei Kang, Nicole R. Donahue, et al.





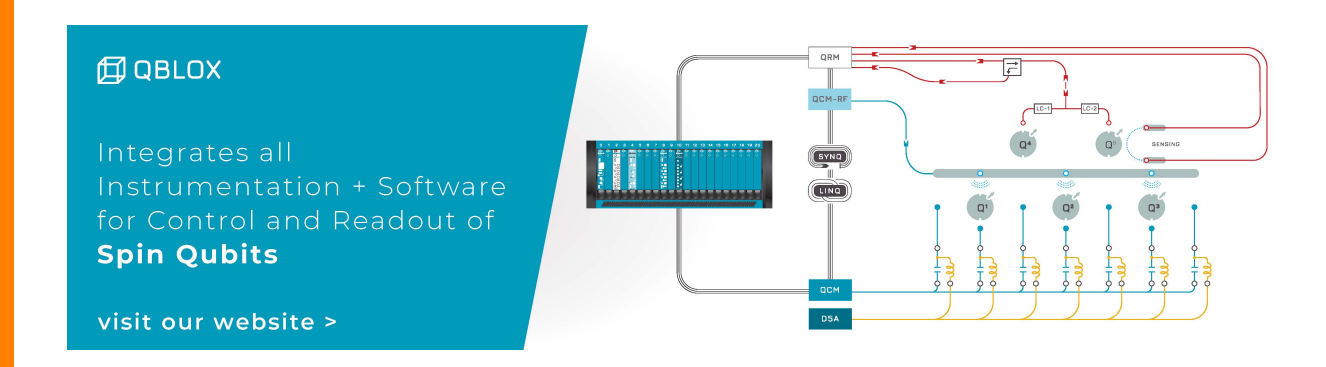


ARTICLES YOU MAY BE INTERESTED IN

A metamaterial sensor for detecting the location of a sub-wavelength object Applied Physics Letters 120, 181703 (2022); https://doi.org/10.1063/5.0090146

Elastic valley Hall phases in bilayer phononic crystal Applied Physics Letters 120, 191702 (2022); https://doi.org/10.1063/5.0091778

Highly efficient UV detection in a metal-semiconductor-metal detector with epigraphene Applied Physics Letters 120, 191101 (2022); https://doi.org/10.1063/5.0090219





3D printed metamaterial absorbers for mid-infrared surface-enhanced spectroscopy

Cite as: Appl. Phys. Lett. **120**, 191703 (2022); doi: 10.1063/5.0093332 Submitted: 28 March 2022 · Accepted: 2 May 2022 ·







Published Online: 11 May 2022

Albanie K. Hendrickson-Stives, 1 (b) Lei Kang, 2,a) (c) Nicole R. Donahue, 1 Christine D. Keating, 1,a) (d) and Douglas H. Werner^{2,a}) (d)

AFFILIATIONS

- ¹Department of Chemistry, The Pennsylvania State University, University Park, Pennsylvania 16802, USA
- ²Department of Electrical Engineering and Center for Nanoscale Science, The Pennsylvania State University, University Park, Pennsylvania 16802, USA
- ^{a)}Authors to whom correspondence should be addressed: lzk12@psu.edu; keating@chem.psu.edu; and dhw@psu.edu

ABSTRACT

The resonant nature and geometric scalability make metamaterials an ideal platform for an enhanced light-matter interaction over a broad frequency range. The mid-infrared (IR) spectral range is of great importance for vibrational spectroscopy of molecules, while IR metamaterials created from lithography-based planar nanostructures have been used to demonstrate enhanced molecular detection. Compared with visible and near-infrared, the relative long wavelengths of IR light make it possible to achieve three-dimensional (3D) IR metamaterials via the state-of-the-art 3D fabrication techniques. Here, we design and fabricate a 3D printed plasmonic metamaterial absorber (MMA), and by performing Fourier-transform IR spectroscopy, we demonstrate that a series of molecular fingerprint vibrations of glycine can be significantly enhanced by the high absorption mode supported by the 3D meta-atoms of the MMA. The observed enhanced IR detection can also be partially attributed to the improved accessibility offered by the 3D architecture of the MMA. In particular, due to capillary forces during the drying process, the microscale 3D printed features lead to selective analyte deposition in high-field regions, which provides another degree of freedom in the design of the 3D printed structures for surface-enhanced IR detection. Our study shows the flexibility of metastructures based on advanced 3D printing technology in tailoring the interaction between IR light and materials on a subwavelength scale.

Published under an exclusive license by AIP Publishing. https://doi.org/10.1063/5.0093332

The development of artificial structures, such as metamaterials and metasurfaces, offers unprecedented opportunity in tailoring the light–matter interaction on subwavelength scales. Importantly, the resonant nature of meta-atoms, i.e., the subwavelength building blocks, makes it possible to achieve enormously enhanced optical fields at the given frequencies or in the predetermined bands. In particular, surface plasmon resonances (SPRs) associated with the coherent oscillations of the electron density induced by an electromagnetic field can result in strong field concentration in the vicinity of plasmonic nanostructures. The resonance enabled field enhancement effect observed in meta-atoms not only gives rise to a series of exotic optical phenomena, such as optical magnetism, 1,2 negative refraction, 3 and giant optical chirality, 4 but also provides the basis for the exploration of the enhanced light–matter interaction for nonlinear 5–8 and sensing 9–14 applications.

Given the fact that the resonance properties of meta-atoms (e.g., the resonance frequencies) are highly sensitive to their dielectric environment, meta-devices have been used for refractive index sensing, ^{15,16}

which has led to the detection of CO₂ gas,¹⁷ glucose,¹⁸ etc. More importantly, the coupling between the optical resonances supported by meta-atoms and vibrational modes of molecules makes it possible to detect molecular groups with extremely high sensitivity. In their pioneering work, Neubrech and co-workers demonstrated a huge enhancement of vibrational signals from less than one attomol of molecules attaching to individual gold nanowires exhibiting plasmonic resonances in the mid-infrared (IR) region.¹⁹ Since then, tremendous efforts have been dedicated to the development of nanostructure based optical sensors for enhanced vibrational spectroscopy.^{15,17,20–46} Among these studies, besides gold and silver, graphene,^{25,27,28,32,33,35} doped semiconductors,^{31,38} and phonon-polaritonic materials⁴⁷ have been adopted to create the plasmonic nanoantennas, while all-dielectric sensors have also been investigated.^{17,24}

In the design of nanostructure-based IR sensors for enhanced vibrational spectroscopy, two main factors are generally considered: (i) ensuring the spectral overlap between the optical resonance of the nanostructure and the vibrational modes of interest, and (ii) good

accessibility of the enhanced optical field created by the nanostructures. The geometric scalability of meta-atoms makes the former easy to satisfy, while the latter condition can be improved by using architectures with three-dimensional (3D) features. ^{29,39,43,48–51} It should be noted that given the wavelengths of interest for vibrational spectroscopy, state-of-the-art 3D-printing techniques based on 3D laser lithography, which is capable of fabricating highly complex 3D structures with sub-micrometer-scale characteristic dimensions, can be exploited to realize 3D metamaterials for IR detection. ⁵² Importantly, compared with the planar structures that are based on conventional lithography methods, 3D printed metamaterials can be readily accessible IR platforms for vibrational molecular spectra.

In this work, by employing 3D printing techniques, we fabricate a 3D metamaterial absorber (MMA) and experimentally demonstrate the large enhancement of the vibrational signals from glycine molecules on the metamaterial. In particular, by introducing glycine onto the fabricated MMA via a solution drop-casting/drying procedure, we identify a series of fingerprint vibrational modes of glycine from the reflection spectra of the system in the wavelength range from 6 to $20~\mu m$. Note that, due to the small amount of glycine involved, most of these spectral features are not detectable from a system where the dry glycine is located on an unpatterned gold film. Our work indicates that 3D printed metamaterials hold great promise for IR detection with significantly enhanced accessibility and improved detection sensitivity.

The proposed 3D printed MMA was fabricated via a two-photon polymerization process. While the details of this Nanoscribe-based 3D-printing approach have been discussed in previous work, 52 a schematic of the corresponding fabrication process is illustrated in

Figs. 1(a) and 1(b). In particular, photoresist-based dielectric split ring resonators (SRRs) on top of an ITO-coated glass coverslide were first obtained by a programmed direct laser writing and developing process and then sputter coated with a 10-nm-thick chromium adhesion layer and a 100-nm-thick gold layer (see the supplementary material for a discussion of the fabrication process). We note that because the thickness of the gold coating is significantly larger than the skin-depth of gold at the operating wavelength, the dielectric property of the photoresist has no influence on the optical response of the proposed metamaterial absorbers. An earlier study at THz frequencies has shown the 3D SRR based design as a good candidate for 3D all-metal metamaterial absorbers.⁵³ A schematic of the 3D printed MMA for IR detection is shown in Fig. 1(c), while SEM images of the fabricated samples are shown in Fig. 1(d). Strong field enhancement and excellent accessibility offered by the 3D printed MMAs can enable IR surface-enhanced spectroscopy with improved sensitivity. We note that, as the gold coating is optically thick for the IR light of interest, the dielectric properties of the photoresist have negligible influence on the absorption response of the MMA samples. Furthermore, the conformal gold coating also ensures zero transmissivity, i.e., the absorptance satisfies $A = 1 - R_{\text{total}}$, where R_{total} represents the total reflectance. For wavelengths longer than 7 μ m (periodicity), $R_{\text{total}} = R_0$, where R_0 is the reflectance of the zero-order reflected wave, while, for the wavelengths shorter than 7 μ m, $R_{\text{total}} = R_0 + \sum R_{(m,n)}$, where $R_{(m,n)}$ corresponds to the reflectance of diffractive waves $(m = 0, \pm 1; n = 0, \pm 1)$.

To study the IR absorption characteristics of the proposed MMAs, we first performed full-wave simulations using the commercial finite integration package CST Microwave Studio. Figure 2(a)

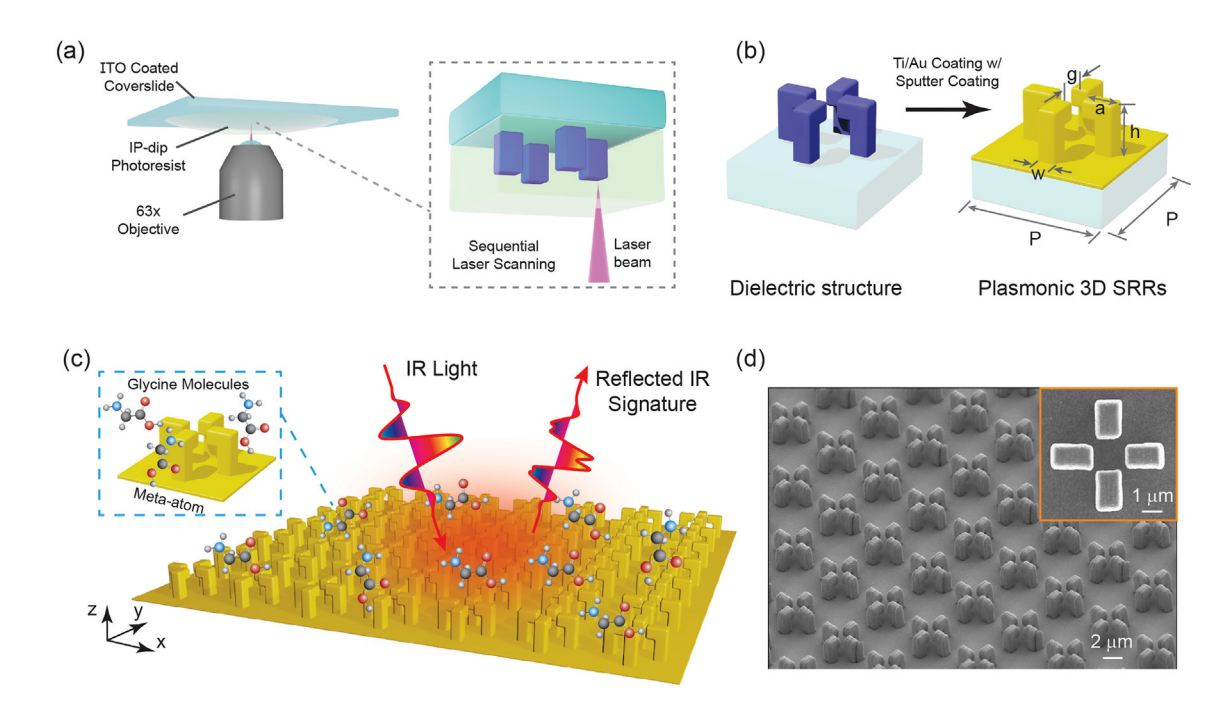


FIG. 1. 3D-printed metamaterial absorbers (MMAs) for mid-infrared surface-enhanced spectroscopy. (a) Schematic of the 3D printing technique based on two-photon polymerization of a negative-tone photoresist. (b) Creating the unit cell structure by gold coating the post-printed 3D SRRs using sputter coating. Geometrical parameters: $P=7~\mu\text{m}$, $h=2.9~\mu\text{m}$, $a=1.7~\mu\text{m}$, $w=1~\mu\text{m}$, and $g=1.5~\mu\text{m}$. (c) IR light reflected from the analyte attached MMA carries information of its molecular fingerprint vibrations. (d) SEM image of the fabricated sample, with the inset illustrating an enlarged SEM image of a unit cell.

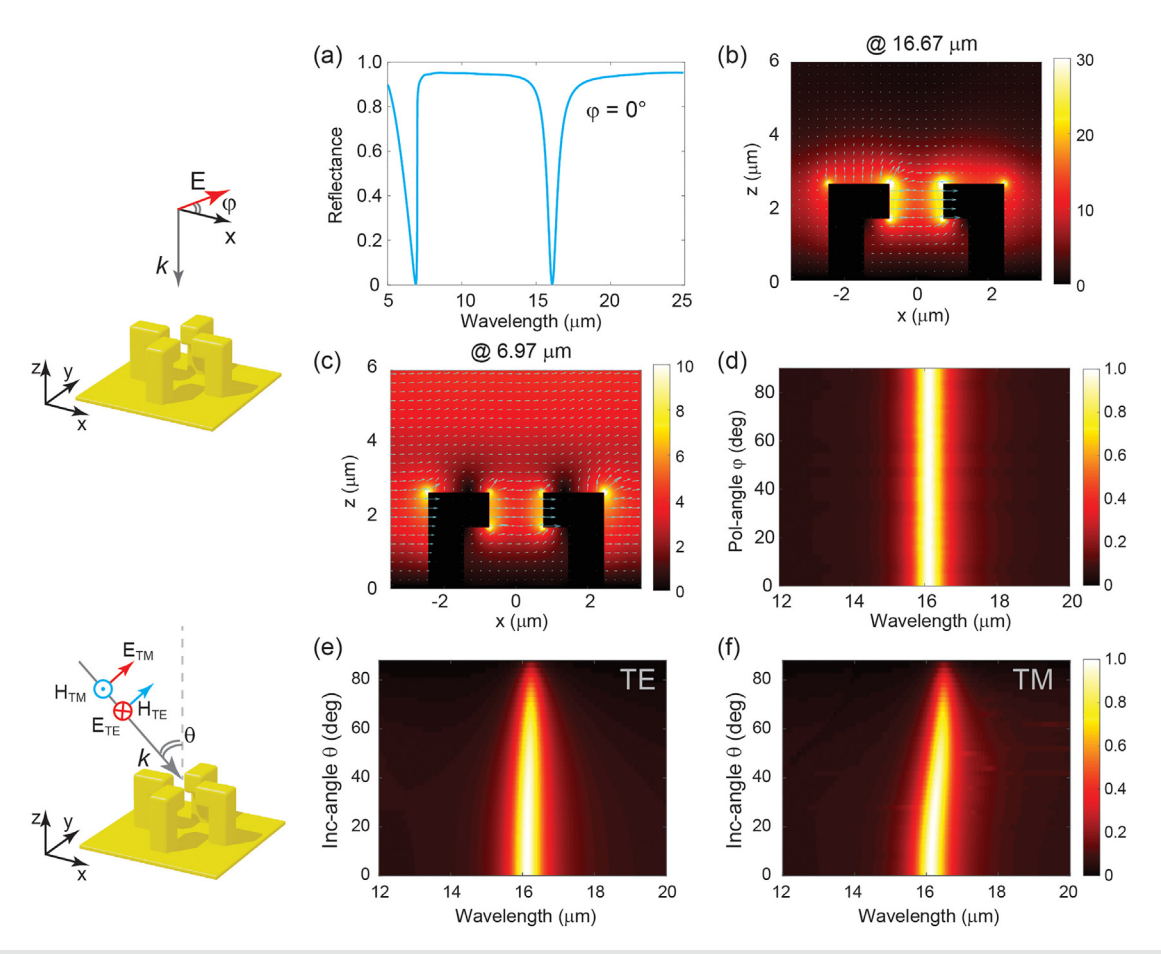


FIG. 2. Simulated response of the MMA. (a) Reflection spectra of the zero-order reflected wave at normal incidence for a polarization angle $\varphi=0$. Schematic of the MMA under illumination of a linearly polarized wave at normal incidence. The corresponding electric field distributions and the associated vector arrows on the y=0 plane at a resonance wavelength of (b) 16.67 μ m and (c) 6.97 μ m, respectively. The electric field magnitude is normalized to that of the incident wave. (d) Simulated absorption as a function of the polarization angle at normal incidence. The incident angular dependence of absorption in the MMA for (e) transverse electric (TE) and (f) transverse magnetic (TM) polarized illumination. Schematic of the oblique incidence is illustrated on the left.

illustrates the simulated reflectance spectrum (R_0) of the MMA at normal incidence when $\varphi = 0$, where φ denotes the polarization angle of the incident wave (see the schematic on the left). Note that the reflection spectra of all diffraction orders are summarized in Fig. S2 in the supplementary material. A sharp reflectance dip is identified at a wavelength of 16.67 μ m, indicating the near-unity absorption of the MMA associated with the pronounced field concentration. This is made evident from the simulated electric field distribution on the y=0 plane shown in Fig. 2(b) in which a maximum field enhancement factor of 30 is observed in the vicinity of the gap of the SRRs. Furthermore, the other sharp reflectance dip identified in Fig. 2(a) at a wavelength of 6.97 μ m can be attributed to the lattice resonance of the periodic structure, resulting in a maximum field enhancement factor of 10 [Fig. 2(c)]. The observed field concentration phenomena imply the potential of the proposed MMA for surface-enhanced spectroscopy. As verified by the simulated results shown in Fig. 2(d), due to the C₄ rotational symmetry of its unit cell, the MMA exhibits optical responses independent of the polarization of the normally incident

light. Moreover, as summarized in Figs. 2(e) and 2(f), for both TE and TM polarized illumination (see schematic of the oblique incidence on the left), the absorption in the MMA is insensitive to the incidence angle ($\theta_{\rm in}$) up to $\sim 30^\circ$. These characteristics of the proposed MMA, i.e., the polarization nonselectivity and incidence angle insensitivity, would be beneficial in practical IR detection applications.

Reflectance spectra were collected using a Fourier transform infrared (FTIR) coupled microscope with a 15× Cassegrain reflective objective (see the supplementary material for more discussions about the reflectance measurements). Experimental data were normalized to an optically thick unpatterned gold film. Figure 3 shows the measured response of the fabricated MMA sample. It can be seen that, when the polarization angle $\varphi = 0^{\circ}$, a sharp reflectance dip is identified at a wavelength of 15.86 μ m, while a low reflectance band can be seen in the wavelength range from 5 to 8 μ m. By rotating a linear polarizer in front of the sample, we measured the response of the MMA sample as a function of φ and summarized the results in Fig. 3(b). It can be seen

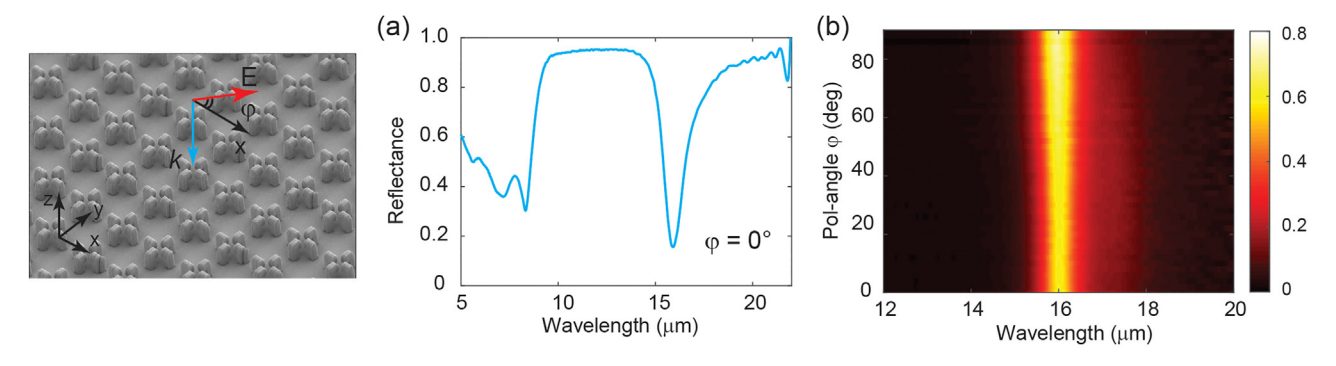


FIG. 3. Measured response of the MMA. (a) Reflection spectra at normal incidence when the polarization angle $\varphi = 0$. (b) Measured absorption as a function of the polarization angle at normal incidence.

that the experimental results are in good agreement with simulations, with moderate discrepancies primarily arising from two factors: (i) fabrication imperfections, and (ii) the off-normal incidence effect due to the finite numerical aperture (N.A.) of the reflective objective used. These measured results indicate the potential of our 3D printed MMAs for surface-enhanced IR detection.

To elucidate the MMA enabled enhanced IR spectroscopy, we introduced glycine into the metamaterial and collected the corresponding reflection spectrum of the system. Glycine, MW 75.07 g/mol, is the simplest biological amino acid and was selected as the analyte because of its series of vibrational modes in the wavelength range of interest. As depicted in Figs. 4(a) and 4(b), the 7 mM glycine/water solution was drop-cast on to the fabricated MMA samples and left to dry in air (see the supplementary material for details). For comparison purposes, the glycine on the bare, unpatterned gold surface was also prepared using the same procedure. Figures 4(c) and 4(d) illustrate the SEM images of the MMA sample before and after the dropcasting/drying procedure, clearly showing that the glycine has been deposited in small "mounds" in the bottom center of the meta-atom. This glycine accumulation phenomenon likely arises from how the microscale 3D printed features impact drying of the glycine solution, influencing both capillary flow and surface tension ("capillarity guided patterning"). 54-57 Hence, the 3D printed features serve not only as MMA resonators but also as microscale collectors concentrating the analyte into an optimal position with a strong field enhancement for detection.

The reflectance spectrum of the MMA after glycine molecule assembly formation is shown in Fig. 4(e) as the red curve, while, for comparison, the reflectance spectra of the corresponding bare MMA are also presented (blue curve). It can be seen that the introduction of glycine in the MMA sample leads to a $\sim 1~\mu m$ redshift of the primary resonance around a wavelength $\sim 16~\mu m$, with a concomitant resonance broadening. These observations can be attributed to the local refractive index changes in the surrounding dielectric matrix. More importantly, a series of spectral features are identified in the reflection spectrum of the glycine/MMA system. To better understand these spectral features, the standard IR reference spectrum of glycine in which the transmittance dips indicate glycine's IR molecular vibration signatures is plotted in Fig. 4(e) as the dashed gray curve. Second A close comparison shows that each spectral feature identified in the red curve

corresponds to a dip seen in the IR reference spectrum of glycine. In particular, at the wavelength of \sim 16.5 μ m, a bump identified in the broad reflectance dip of the glycine/MMA system is found to correspond to the "COOH bend" and "NCCO bend" vibration mode. From the standpoint of the MMA, the corresponding molecular vibration of glycine increases the loss of the surrounding dielectric matrix and has negative influence on the perfect absorption mode of the MMA, resulting in the increase in reflectance at the frequency. On the other hand, relative to the bare-MMA, other molecular vibration modes of glycine in the frequency range of interest are significantly enhanced by the MMA and give rise to the higher system absorption, leading to a series of reflectance dips (e.g., at wavelengths \sim 9, 11, and 20 μ m) in the red curve. It is important to note that, in stark contrast, most of these IR signatures are not detectable from the reflectance spectrum of dry glycine on the unpatterned gold film [orange curve in Fig. 4(e)]. These results unambiguously demonstrate the feasibility of the 3D printed MMAs for highly sensitive IR detection of molecules.

In summary, we have demonstrated a 3D printed metamaterial absorber for mid-infrared surface-enhanced spectroscopy. By performing FTIR spectroscopy, we have shown that the fabricated absorber based on a state-of-the-art 3D fabrication technique exhibits polarization-insensitive strong IR absorption at a wavelength of \sim 16 μ m. Furthermore, by introducing glycine into the fabricated metamaterial samples using a drop-casting/drying procedure, we have demonstrated that a series of molecular fingerprint vibrations of glycine can be clearly identified from the reflectance spectrum of the system. Note that, due to the small amount of glycine involved, those IR vibration modes are generally undetectable on an unpatterned surface. The observed enhanced IR detection is primarily based on the strong optical resonances supported by the proposed metamaterial absorbers, which significantly increase the light-matter interaction between analytes and IR light. In addition, compared with planar structures, the improved accessibility offered by the 3D printed architectures allows analytes to access the highly concentrated field in the vicinity of metaatoms. Importantly, due to capillary flow and surface tension, the microscale 3D printed features have significant influences on the solute deposition, which provides another degree of freedom in the design of the 3D printed structures for surface-enhanced IR detection. Although the selective deposition of analyte in a high-sensitivity

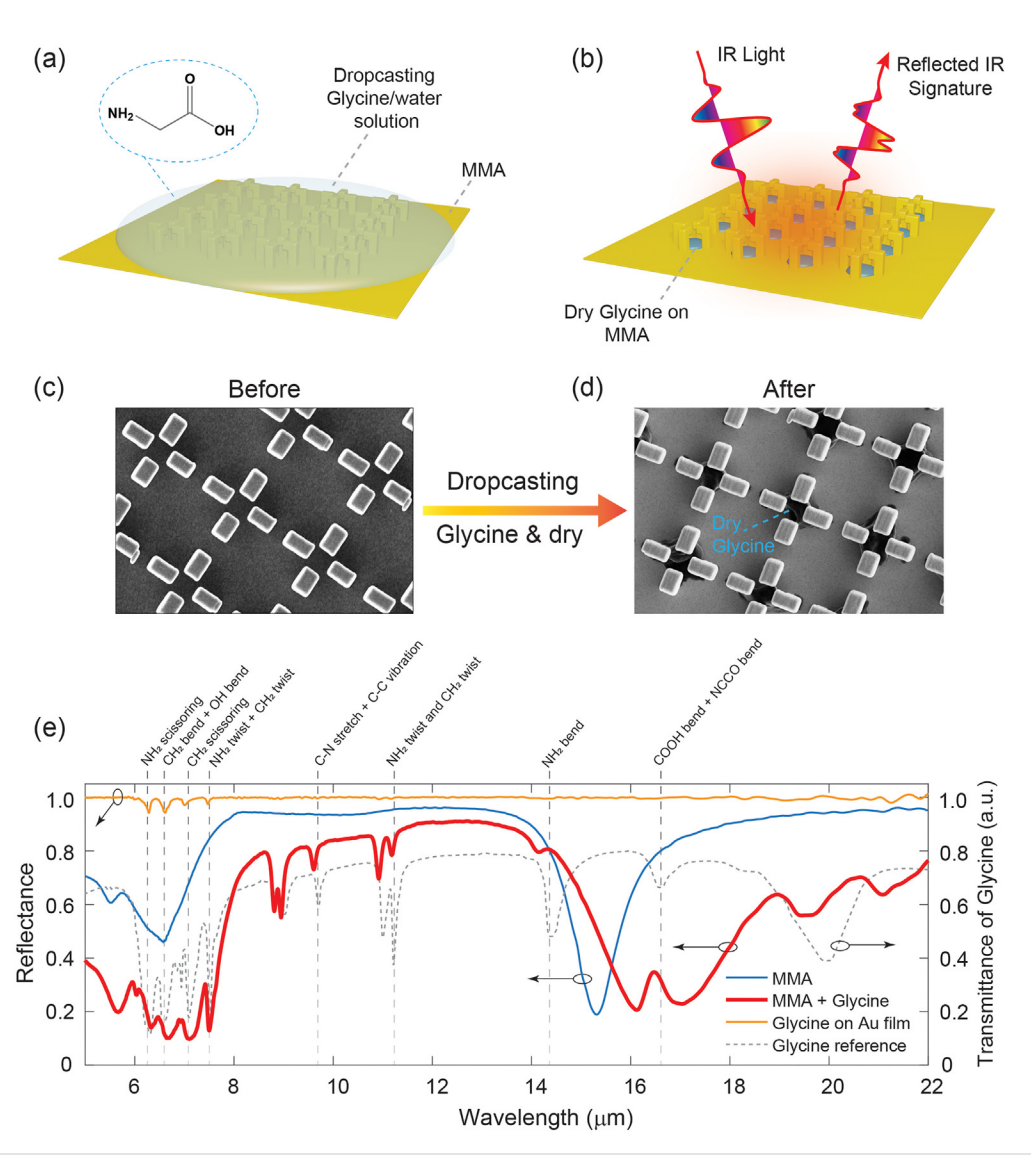


FIG. 4. MMA enabled enhanced infrared reflection spectroscopy of glycine. Schematic of (a) drop-casting glycine-water solution (7 mM) on the MMA for (b) IR detection after drying in air. SEM images (c) before and (d) after the drop-casting and drying procedure. Glycine prefers to dry in the center of the unit cells. (e) Reflection spectrum of the glycine-attached MMA (red curve). For comparison purposes, the reflection spectra of the MMA without glycine (blue), and the dry glycine on unpatterned gold film (orange) are also presented. The standard transmission spectrum of glycine (dashed gray) is provided as a reference.

location was a serendipitous outcome in this study, in the future, 3D printed metamaterials could be designed with capillarity-guided deposition patterning in mind to optimize performance. Our study shows the potential of 3D printed IR metamaterials for applications of chemical and biochemical substances sensing.

See the supplementary material for more discussion of device fabrication, optical characterization, and numerical simulations.

This research was supported by the Penn State Materials Research Science and Engineering Center (MRSEC, Grant No. NSF DMR-1420620) and by the Penn State University Office of the President/Executive Vice President & Provost.

AUTHOR DECLARATIONS Conflict of Interest

The authors have no conflicts to disclose.

Author Contributions

A.K.H.-S. and L.K. contributed equally to this work.

DATA AVAILABILITY

The data that support the findings of this study are available from the corresponding authors upon reasonable request.

REFERENCES

- ¹H.-K. Yuan, U. K. Chettiar, W. Cai, A. V. Kildishev, A. Boltasseva, V. P. Drachev, and V. M. Shalaev, Opt. Express 15, 1076 (2007).
- ²J. C. Ginn, I. Brener, D. W. Peters, J. R. Wendt, J. O. Stevens, P. F. Hines, L. I. Basilio, L. K. Warne, J. F. Ihlefeld, P. G. Clem, and M. B. Sinclair, Phys. Rev. Lett. 108, 097402 (2012).
- ³J. Valentine, S. Zhang, T. Zentgraf, E. Ulin-Avila, D. A. Genov, G. Bartal, and X. Zhang, Nature 455, 376 (2008).
- ⁴J. K. Gansel, M. Thiel, M. S. Rill, M. Decker, K. Bade, V. Saile, G. von Freymann, S. Linden, and M. Wegener, Science **325**, 1513 (2009).
- ⁵G. Li, S. Zhang, and T. Zentgraf, Nat. Rev. Mater. 2, 17010 (2017).
- ⁶A. Krasnok, M. Tymchenko, and A. Alù, Mater. Today 21, 8 (2018).
- ⁷N. M. Litchinitser, Adv. Phys.-X 3, 1367628 (2018).
- ⁸E. Rahimi and R. Gordon, Adv. Opt. Mater. **6**, 1800274 (2018).
- ⁹Y. Zhang, W. Chu, A. D. Foroushani, H. Wang, D. Li, J. Liu, C. J. Barrow, X. Wang, and W. Yang, Materials 7, 5169 (2014).
- ¹⁰B. Špačková, P. Wrobel, M. Bocková, and J. Homola, Proc. IEEE 104, 2380 (2016).
- ¹¹S. Kasani, K. Curtin, and N. Wu, Nanophotonics **8**, 2065 (2019).
- ¹²V. Krivenkov, S. Goncharov, I. Nabiev, and Y. P. Rakovich, Laser Photonics Rev. 13, 1800176 (2019).
- ¹³M. Seo and H.-R. Park, Adv. Opt. Mater. **8**, 1900662 (2020).
- ¹⁴S.-H. Oh, H. Altug, X. Jin, T. Low, S. J. Koester, A. P. Ivanov, J. B. Edel, P. Avouris, and M. S. Strano, Nat. Commun. 12, 3824 (2021).
- ¹⁵I. M. Pryce, Y. A. Kelaita, K. Aydin, and H. A. Atwater, ACS Nano 5, 8167 (2011).
- ¹⁶N. Verellen, P. Van Dorpe, C. Huang, K. Lodewijks, G. A. E. Vandenbosch, L. Lagae, and V. V. Moshchalkov, Nano Lett. 11, 391 (2011).
- ¹⁷Y. Chang, D. Hasan, B. Dong, J. Wei, Y. Ma, G. Zhou, K. W. Ang, and C. Lee, ACS Appl. Mater. Interfaces 10, 38272 (2018).
- ¹⁸M. Mesch, C. Zhang, P. V. Braun, and H. Giessen, ACS Photonics 2, 475 (2015).
- 19 F. Neubrech, A. Pucci, T. W. Cornelius, S. Karim, A. García-Etxarri, and J. Aizpurua, Phys. Rev. Lett. 101, 157403 (2008).
- ²⁰B. Lahiri, A. Z. Khokhar, R. M. De La Rue, S. G. McMeekin, and N. P. Johnson, Opt. Express 17, 1107 (2009).
- ²¹E. Cubukcu, S. Zhang, Y.-S. Park, G. Bartal, and X. Zhang, Appl. Phys. Lett. 95, 043113 (2009).
- ²²F. Neubrech, D. Weber, D. Enders, T. Nagao, and A. Pucci, J. Phys. Chem. C 114, 7299 (2010).
- ²³A. A. Yanik, A. E. Cetin, M. Huang, A. Artar, S. H. Mousavi, A. Khanikaev, J. H. Connor, G. Shvets, and H. Altug, Proc. Natl. Acad. Sci. U. S. A. 108, 11784 (2011)
- ²⁴S. Law, L. Yu, A. Rosenberg, and D. Wasserman, Nano Lett. **13**, 4569 (2013).
- ²⁵B. Vasić, G. Isić, and R. Gajić, J. Appl. Phys. **113**, 013110 (2013).
- ²⁶H. Aouani, H. Šípová, M. Řahmani, M. Navarro-Cia, K. Hegnerová, J. Homola, M. Hong, and S. A. Maier, ACS Nano 7, 669 (2013).
- ²⁷Y. Li, H. Yan, D. B. Farmer, X. Meng, W. Zhu, R. M. Osgood, T. F. Heinz, and P. Avouris, Nano Lett. 14, 1573 (2014).
- ²⁸Y. Francescato, V. Giannini, J. Yang, M. Huang, and S. A. Maier, ACS Photonics 1, 437 (2014).

- ²⁹ A. E. Cetin, D. Etezadi, and H. Altug, Adv. Opt. Mater. 2, 866 (2014).
- ³⁰D. Rodrigo, O. Limaj, D. Janner, D. Etezadi, F. de Abajo, V. Pruneri, and H. Altug, Science 349, 165 (2015).
- ³¹L. Baldassarre, E. Sakat, J. Frigerio, A. Samarelli, K. Gallacher, E. Calandrini, G. Isella, D. J. Paul, M. Ortolani, and P. Biagioni, Nano Lett. 15, 7225 (2015).
- ³²I. J. Luxmoore, P. Q. Liu, P. Li, J. Faist, and G. R. Nash, ACS Photonics 3, 936 (2016).
- ³³L. Zundel and A. Manjavacas, ACS Photonics **4**, 1831 (2017).
- ³⁴X. Chen, C. Wang, Y. Yao, and C. Wang, ACS Nano 11, 8034 (2017).
- 35T. Wu, Y. Luo, and L. Wei, Opt. Lett. 42, 2066 (2017).
- ³⁶G. Dayal, A. Solanki, X. Y. Chin, T. C. Sum, C. Soci, and R. Singh, J. Appl. Phys. 122, 073101 (2017).
- ³⁷D. Ji, A. Cheney, N. Zhang, H. Song, J. Gao, X. Zeng, H. Hu, S. Jiang, Z. Yu, and Q. Gan, Adv. Opt. Mater. 5, 1700223 (2017).
- ⁵⁸F. B. Barho, F. Gonzalez-Posada, M.-J. Milla, M. Bomers, L. Cerutti, E. Tournié, and T. Taliercio, Nanophotonics 7, 507 (2017).
- ³⁹I. Hwang, J. Yu, J. Lee, J.-H. Choi, D.-G. Choi, S. Jeon, J. Lee, and J.-Y. Jung, ACS Photonics 5, 3492 (2018).
- ⁴⁰D. Rodrigo, A. Tittl, A. John-Herpin, O. Limaj, and H. Altug, ACS Photonics 5, 4903 (2018).
- ⁴¹L. Kühner, R. Semenyshyn, M. Hentschel, F. Neubrech, C. Tarín, and H. Giessen, ACS Sens. 4, 1973 (2019).
- ⁴²D. Li, H. Zhou, X. Hui, X. He, H. Huang, J. Zhang, X. Mu, C. Lee, and Y. Yang, Adv. Sci. 8, 2101879 (2021).
- ⁴³I. Hwang, M. Kim, J. Yu, J. Lee, J.-H. Choi, S. A. Park, W. S. Chang, J. Lee, and J.-Y. Jung, Small Methods 5, 2100277 (2021).
- ⁴⁴G. Armelles, L. Bergamini, A. Cebollada, N. Zabala, and J. Aizpurua, J. Appl. Phys. 129, 073103 (2021).
- 45T. Zhang, D. He, L. Liu, Q. Wulan, J. Yu, Z. Li, and Z. Liu, AIP Adv. 11, 035305 (2021).
- ⁴⁶X. Miao, L. Yan, Y. Wu, and P. Q. Liu, Light **10**, 5 (2021).
- ⁴⁷M. Autore, I. Dolado, P. Li, R. Esteban, F. J. Alfaro-Mozaz, A. Atxabal, S. Liu, J. H. Edgar, S. Vélez, F. Casanova, L. E. Hueso, J. Aizpurua, and R. Hillenbrand, Adv. Opt. Mater. 9, 2001958 (2021).
- ⁴⁶X. Xiong, S.-C. Jiang, Y.-H. Hu, R.-W. Peng, and M. Wang, Adv. Mater. **25**, 3994 (2013).
- ⁴⁹I. Sakellari, X. Yin, M. L. Nesterov, K. Terzaki, A. Xomalis, and M. Farsari, Adv. Opt. Mater. 5, 1700200 (2017).
- ⁵⁰S. K. Saha, D. Wang, V. H. Nguyen, Y. Chang, J. S. Oakdale, and S.-C. Chen, Science 366, 105 (2019).
- ⁵¹J. Reinbold, T. Frenzel, A. Münchinger, and M. Wegener, Materials 12, 3527 (2019).
- ⁵²N. R. Famularo, L. Kang, Z. Li, T. Zhao, K. L. Knappenberger, C. D. Keating, and D. H. Werner, J. Chem. Phys. 153, 154702 (2020).
- ⁵³M. Wu, X. Zhao, J. Zhang, J. Schalch, G. Duan, K. Cremin, R. D. Averitt, and X. Zhang, Appl. Phys. Lett. 111, 051101 (2017).
- ⁵⁴M. Kang, W. Park, S. Na, S.-M. Paik, H. Lee, J. W. Park, H.-Y. Kim, and N. L. Jeon, Small 11, 2789 (2015).
- ⁵⁵J. Bae, J. Lee, Q. Zhou, and T. Kim, Adv. Mater. **31**, 1804953 (2019).
- ⁵⁶N. A. Dudukovic, E. J. Fong, H. B. Gemeda, J. R. DeOtte, M. R. Cerón, B. D. Moran, J. T. Davis, S. E. Baker, and E. B. Duoss, Nature 595, 58 (2021).
- ⁵⁷B. Lee, S. Kim, J. Ko, S.-R. Lee, Y. Kim, S. Park, J. Kim, S. Hyung, H.-Y. Kim, and N. L. Jeon, NPG Asia Mater. 14, 6 (2022).
- 58C. D. Craver, The Coblentz Society Desk Book of Infrared Spectra, 2nd ed. (The Coblentz Society, Kirkwood, MO, 1982).